Anisotropic Molecular Organization at Liquid/Vapor Interface Promotes Crystal Nucleation with Polymorph Selection

Xin Yao[1], Qitong Liu[2], Bu Wang[2], Junguang Yu[1], Michael M. Aristov[3], Chenyang Shi[4,5], Geoff G. Z. Zhang[4,*], Lian Yu[1,3,*]

[1] School of Pharmacy, University of Wisconsin-Madison, Madison, WI, 53705, USA

[2] Civil & Environmental Engineering, University of Wisconsin-Madison, Madison, WI, 53705, USA

[3] Department of Chemistry, University of Wisconsin-Madison, Madison, WI, 53705, USA

[4] Drug Product Development, Research and Development, AbbVie Inc., North Chicago, IL, 60064, USA

[5] Current address: Data Science Consulting, Tiger Analytics, Santa Clara, CA, 95054, USA

Abstract. The molecules at the surface of a liquid have different organization and dynamics from those in the bulk, potentially altering the rate of crystal nucleation and polymorphic selection, but this effect remains poorly understood. We present the first demonstration that nucleation at the surface of a pure liquid, D-arabitol, is vastly enhanced, by 12 orders of magnitude, and selects a different polymorph. The surface effect intensifies with cooling and can be inhibited by a dilute, surface-active second component. This phenomenon arises from the anisotropic molecular packing at the interface and its similarity to the surface-nucleating polymorph. Our finding is relevant for controlling the crystallization and polymorphism in any system with a significant interface such as nanodroplets and atmospheric water.

Introduction

Crystal nucleation is important in many areas of science and technology,[1-5] but important unanswered questions remain.[6] One such question concerns the effect of a liquid/vapor interface on nucleation, which is relevant for understanding ice formation from atmospheric water[7] and the crystallization of metallic nano-droplets,[8, 9] silicon,[10] and organic liquids.[11, 12] There have been reports of interface-induced nucleation with polymorph control[13-15] but surprisingly little is known about the role of the vapor interface of a pure liquid. A liquid/vapor interface has a different structure from the bulk liquid, exhibiting layering,[16, 17] preferred orientation,[18-20] and enhanced mobility.[21, 22] These features potentially alter the nucleation rate, but our understanding of the effect is very limited. According to the Classical Nucleation Theory (CNT),[23] the rate of nucleation depends on the thermodynamic barrier to create a new interface and the molecular mobility available, and both factors are modified by the interfacial environment. It is difficult, however, to use the CNT to make quantitative predictions because of the unknown parameters in the theory. Surface-initiated crystal nucleation has been observed by simulations,[8-10] the results are generally obtained for nanodroplets or thin films and are often sensitive to the force fields used.[24-26] To our knowledge, there has been no experimental demonstration that a single-component liquid can have different nucleation rates in the bulk and at the surface. In the case of water, there is considerable interest[7] and ongoing debate over the role of surface water on ice crystallization.[27] Given the importance of crystal polymorphs and their control,[28] a further question in this area is whether surface nucleation selects a different polymorph from the bulk nucleation.

Here we report the first experimental demonstration where nucleation at the liquid/vapor interface is vastly enhanced, by 12 orders of magnitude, and selects a different polymorph. This phenomenon arises from the similarity of the surface molecular packing to the surface-nucleating polymorph and can be inhibited by a dilute, surface-active second component. Our results demonstrate that the anisotropic molecular packing at an interface can significantly alter both the rate and the polymorph of nucleation.

Results and Discussion

Crystal Structures and Molecular Conformations of D-Arabitol. Our model system is D-arabitol (Figure 1), a glass-forming polyol derived from carbohydrates.[29] Polyols have applications in cryoprotection,[30] food and drug formulations, and energy storage.[31] Two polymorphs of D-arabitol are known at present: I[32] and II (structure solved in this work; see the Crystallographic Information File in the SI and Table S1). The polymorphs have similar molecular conformations conforming to Jeffrey's Rule[33] but different molecular packing and hydrogen-bond (HB) networks. As Figure 1 shows, Form I has a 3-dimensional HB network, while Form II consists of 2-dimensional HB layers with no HBs between the layers. As we show later, the structural difference leads to different polymorphic preference of bulk and surface nucleation. Being a chiral molecule, the two termini of D-arabitol (C1 and C5) are inequivalent and the terminal CO group is persistently bent relative to the carbon chain at the C5 end and either bent or extended at the C1 end, consistent with CSD statistics (Table S2).

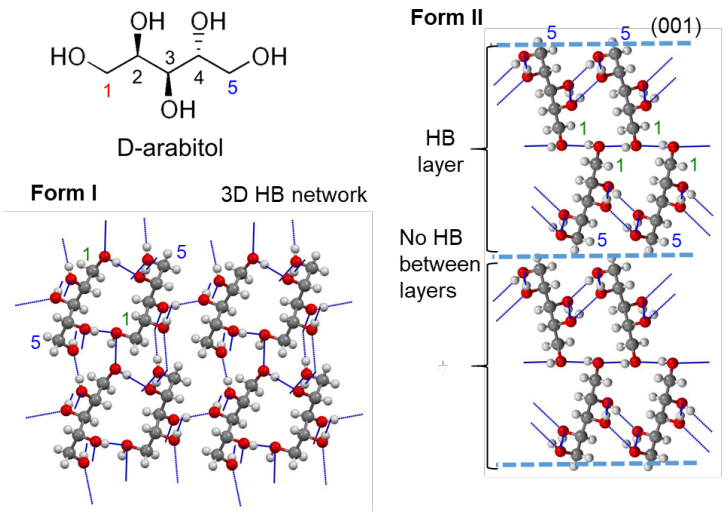

Figure 1. Crystal structures of D-arabitol. Form I has a 3D HB network; Form II has HB layers with no HB between layers. The two termini (C1 and C5) are inequivalent.

Nucleation Rates at the Surface and in the Bulk. To investigate the effect of a liquid/vapor interface on nucleation, we have measured the nucleation rates in the bulk of liquid D-arabitol and at its free surface. In a bulk experiment (Figure 2a), a liquid film is sandwiched between two coverslips and no vapor interface is present in the region of observation. In a surface experiment (Figure 2b), the top coverslip is absent, thus creating a free surface. The sample was protected from moisture with a blanket of dry nitrogen. In both cases, the film thickness was nominally 50 μm and was varied to test the mechanism of nucleation as described below. Figures 2c and 2d show the qualitative difference between the number of crystals created without and with a vapor interface. Each sample was nucleated at 278 K for a chosen time and heated to 323 K for 1 min to

grow the nuclei to visible size. (Without the heating step, or only with the heating step, no crystals were observed indicating nucleation occurred at 278 K.) We find that in the presence of a vapor interface, nucleation was significantly faster: far more crystals nucleated in 10 s in the free-surface sample (Figure 2d) than in 411 min in the bulk sample (2c). Furthermore, by varying the thickness of the open liquid film h from 30 to 240 μm, we observed no significant effect on the number of crystals per surface area, consistent with surface nucleation.

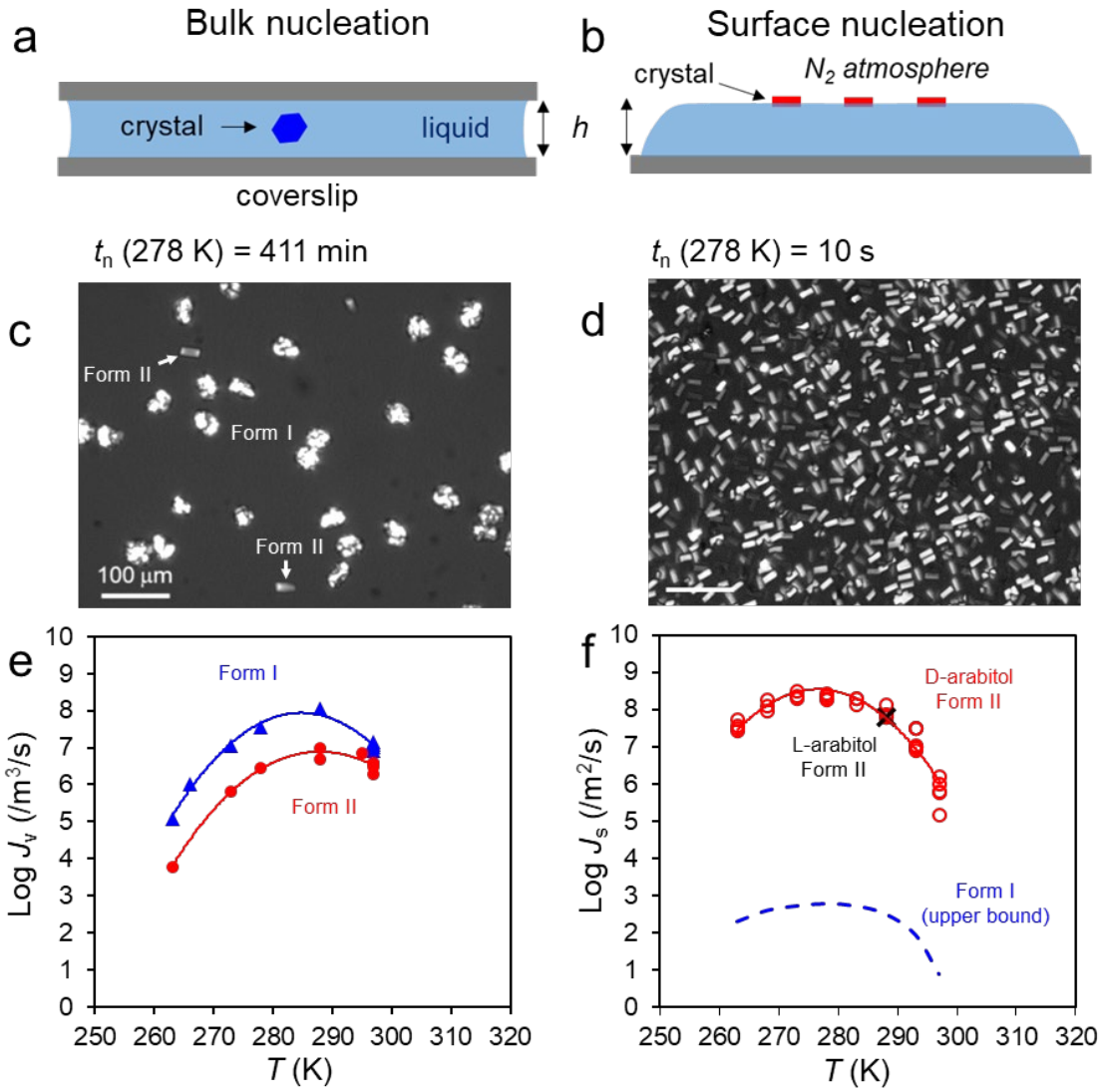

Figure 2. (a, b) Bulk- and surface-nucleation experiments. The thickness of the liquid film h is nominally 50 μm. (c, d) Comparison of the densities of bulk- and surface-nucleated crystals at 278 K. After nucleation at 278 K, each sample spent 60 s at 323 K for the nuclei to grow. Surface nucleation created more crystals in 10 s than bulk nucleation in 411 min. Furthermore, surface nucleation yielded Form II while bulk nucleation mainly Form I (10 % Form II). (e, f) Bulk- and surface-nucleation rates, J_v and J_s, *vs.* temperature. In (f), the black X is a data point for L-arabitol which agrees with the D-isomer value. The curves are guide to the eye.

An important feature of the surface nucleation in D-arabitol is its different polymorphic preference from bulk nucleation. Bulk nucleation produced mainly Form I, with Form II being a minor component (10 %), whereas surface nucleation produced only Form II, with no detectable Form I. The two polymorphs are readily distinguished by their morphologies, melting points (376 K for I and 356 K for II), and X-ray diffraction patterns (Figure 3). The X-ray pattern also indicates that surface-nucleated crystals have a preferred orientation: the observed peaks are all (00*l*) reflections, indicating the (001) plane is parallel to the liquid/vapor interface. Real-time observation of surface crystallization showed no crystal rotation during growth, suggesting that the surface crystals nucleated in the preferred orientation. As we discuss below, this result is consistent with the selective nucleation Form II at the surface.

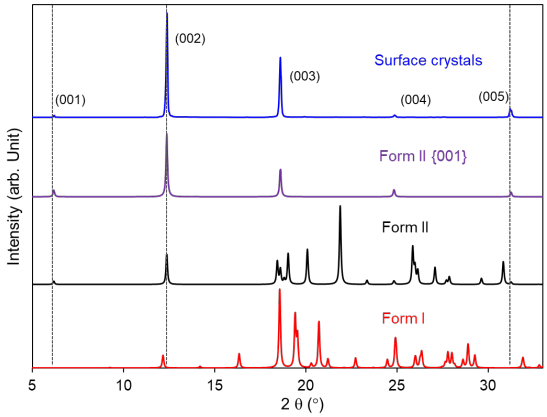

Figure 3. X-ray diffraction pattern of surface-nucleated crystals (top) and predicted patterns of Forms I and II from their crystal structures. The observed pattern matches that of Form II (see the vertical lines indicating peaks unique to Form II) and all the peaks correspond to (00*l*), indicating the (001) plane is parallel to the liquid/vapor interface.

Figures 2e and 2f show the bulk and surface nucleation rates in D-arabitol. The development method[34] was used for this purpose where the number of crystals was measured as a function of nucleation time (see Figure S1 for typical data). We find that in the bulk, Form I nucleates faster than Form II by approximately a factor of 10, whereas at the surface, only Form II nucleates and Form I is never observed. We estimate the surface nucleation of Form I to be at least 5 orders of magnitude slower than that of Form II (dashed curve in Figure 2f). This estimate is based on the non-observation of Form I crystals in all the experiments performed: J_s (Form I) < $1/(A_{total}\ t_{total})$, where A_{total} is the total area of the melt sample examined and t_{total} is the total time of the experiment. In addition to D-arabitol, Figure 2f contains a data point on L-arabitol. Being mirror images of each other, D- and L-arabitol should exhibit the same surface nucleation phenomenon, and this was indeed observed.

The results above indicate a strong surface effect on crystal nucleation. We now show that surface nucleation is vastly faster than bulk nucleation when compared on a per-molecule basis. Because of the different units of J_v (1/m^3/s) and J_s (1/m^2/s), the two rates cannot be compared directly. To compare them, we convert each to the per-molecule value: $J_{v0} = J_v\,\Omega_0$ and $J_{s0} = J_s\,A_0$, where Ω_0 is the volume occupied by one molecule and A_0 is the surface area occupied by one molecule. J_{v0} (J_{s0}) is the number of nucleation events per second in the volume (area) occupied by one molecule. Defined on a per-molecule basis, the values of J_{v0} and J_{s0} are exceedingly small, but this should not cause confusion since the base can be enlarged to one mole of molecules so that J_{v0} (J_{s0}) is the frequency of nucleation per molar volume (molar surface area). For D-arabitol, $\Omega_0 = 0.2$ nm^3 from its bulk density, and $A_0 \approx \Omega_0^{2/3} = 0.3$ nm^2. In Figure 4a, the J_{v0} and J_{s0} values are plotted against temperature, and we observe a large difference between these values for Form II. For example, at 273 K (arrow), $J_{s0}/J_{v0} = 10^{12}$ for Form II, meaning surface nucleation outpaces bulk nucleation by 12 orders of magnitude when compared on a per-molecule basis. In contrast, $J_{s0}/J_{v0} < 10^5$ for Form I. This quantifies the strong polymorphic preference of surface nucleation.

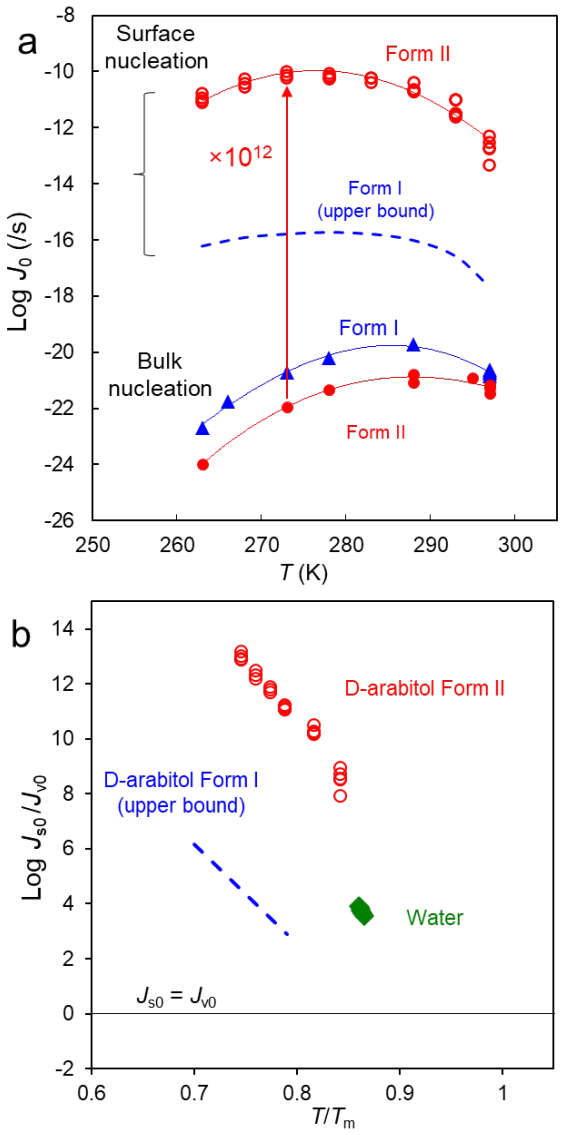

Figure 4. (a) Per-molecule rates of surface and bulk nucleation. Surface nucleation of D-arabitol Form II is vastly faster than bulk nucleation while the difference is smaller for Form I. (b) J_{s0}/J_{v0} ratios for D-arabitol and water, where J_{s0} and J_{v0} are the per-molecule rates of surface and bulk nucleation. The ratio increases with cooling. The horizontal line at bottom indicates the condition that surface and bulk nucleation are equally productive on a per-molecule basis.

In Figure 4b, we plot the surface-enhancement factor J_{s0}/J_{v0} as a function of temperature and compare the result with that of water. For this comparison, the temperature has been scaled by the crystal melting point T_m. The horizontal line indicates the condition $J_{s0} = J_{v0}$, that is, surface and bulk nucleation are equally productive on a per-molecule basis. Above this line, nucleation is enhanced by the surface and below this line, inhibited. For D-arabitol Form II, $J_{s0}/J_{v0} = 10^8 – 10^{13}$ in the temperature range investigated and increases with cooling. This means that surface nucleation is more productive than bulk nucleation at lower temperatures, likely a result of greater surface ordering observed by MD simulations (see below). For water,[35,36] droplets larger than tens of micrometers show predominantly bulk nucleation, whereas surface nucleation is important for micrometer-sized droplets. From these results, Kuhn et al. extracted water's surface and bulk nucleation rates.[36] Their result indicates $J_{s0}/J_{v0} = 10^3 – 10^4$, smaller than the value for D-arabitol Form II and comparable to the upper bound estimated for Form I, and the limited data on water also suggest that the surface-enhancement of nucleation increases with cooling.

A Dilute Surface-Active Component Inhibits Surface Nucleation. The strong effect of a liquid/vapor interface on nucleation suggests an ability to disrupt the process through a second component that is enriched at the interface like a surfactant in water. This effect was indeed observed for D-arabitol doped with polyvinylpyrrolidone (PVP, molecular-weight grade K30). PVP is a polymer miscible with D-arabitol and at low concentrations (<1 %), has no effect on bulk nucleation.[37] We observed, however, that at only 20 ppm (0.0002 wt%), PVP can significantly inhibit surface nucleation and the effect increases with PVP concentration (Figure 5). This effect arises because PVP can enrich at the liquid/vapor interface of D-

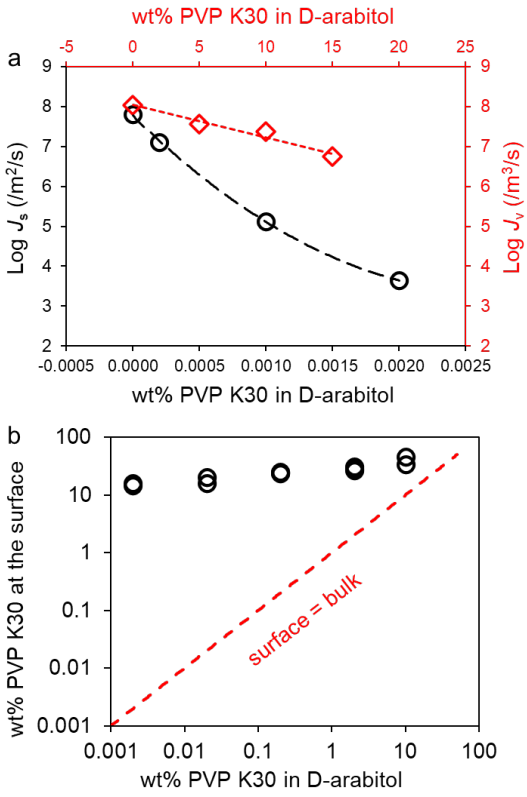

Figure 5. (a) Surface and bulk nucleation rates *vs.* the wt% of PVP K30. Inhibition of surface nucleation occurs at much lower concentrations (lower *x* axis) than that of bulk nucleation (upper *x* axis). (b) wt% of PVP at the surface (measured by XPS) *vs.* wt% of PVP in the bulk, showing a strong surface enrichment effect. The diagonal line indicates the condition of equal surface and bulk concentrations.

arabitol. Using X-ray Photoelectron Spectroscopy (XPS), we determined the surface concentration of PVP (see Figure S2 for typical data).[38] The result (Figure 5b) indicates that the surface concentration of PVP is substantially higher than its bulk concentration, consistent with its greater hydrophobicity and lower surface tension. This would reduce the surface concentration of D-arabitol and its driving force to crystallize. The surface enrichment of PVP could also alter the local structure that promotes surface nucleation. This result confirms our assignment of the nucleation mechanism (via the liquid/vapor interface) and provides a tool to control the process.

It is important to rule out the possibility of surface contamination in the surface nucleation process. Here we summarize the evidence against this possibility. Surface analysis by XPS observed only the elements present in D-arabitol. Throughout the experiment, the sample was sealed in a chamber purged with high-purity nitrogen. We observed uniform distribution of the nuclei on the surface unrelated to the flow direction of nitrogen and longer purging did not alter the nucleation rate. Replacing the nitrogen purge with vacuum (10 mTorr) had no significant effect on the results. The nucleation process showed an extended steady state (Figure S1); had it been catalyzed by contaminants, the nucleation rate should be fast initially but quickly plateau without an extended steady state. The enrichment of PVP at the liquid/vapor interface (Figure 5b) substantially reduced the rate of nucleation (Figure 5a). Different batches of D-arabitol from multiple suppliers and recrystallized by different cycles showed no significant difference in nucleation rate (Figure 2f contains data from different batches). The simplest explanation for this is that all the batches were sufficiently pure and surface nucleation is an intrinsic property of the material.

Structure of Liquid Surface by Molecular Dynamics Simulations. Having established the significant effect of the liquid/vapor interface on nucleation and polymorph selection experimentally, we now investigate the structural origin of the phenomenon by MD simulations. For this purpose, the Force Field (FF) was a modified version of AMBER BCFF (Table S3 and S4), which has been applied with success to the smaller polyol, glycerol.[39] The FF was validated by reproducing the experimental crystal structures (Table S5) and the expected conformers based on crystal structures (Table S2). After equilibration, 84 % of the molecules have the conformations observed in crystals, that is, the carbon backbone is an extended zigzag and the terminal CO is

bent relative to the backbone at C5 and either bent or extended at C1. This provides another validation of our FF.

Figure 6 shows how structure varies across the liquid/vapor interface of D-arabitol. The density profile (Figure 6a) defines the thickness of the liquid film. Figure 6a also shows the probability for each OH group to participate in HB. The HB profile closely matches the density profile, indicating that the molecule forms roughly the same number of HBs in the surface region as in the bulk. This is expected since the HB is the strongest interaction in the liquid and molecules organize themselves to maximize the number of HBs regardless of their physical environment. This conclusion is supported by the preferred orientation of the OH and CO vectors into the film (Figure 6b).

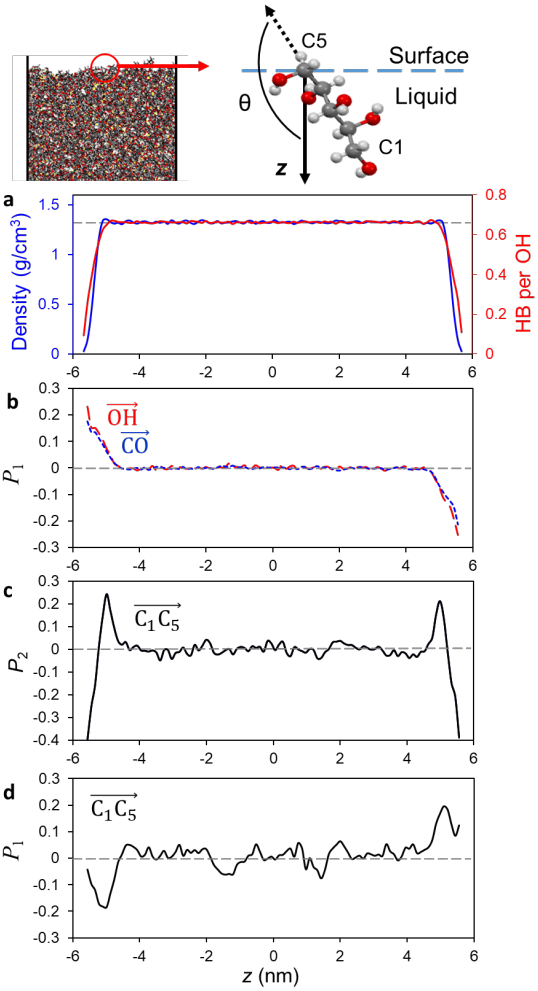

Figure 6. Order parameters vs depth *z*. (a) Density and HB density. (b) P_1 order parameters of the OH and CO vectors. (c, d) P_2 and P_1 order parameters of the C_1C_5 vector.

In Figure 6b, we plot the order parameter $P_1 = <\cos\phi>$ for the angle ϕ between the OH or CO vector and the surface normal. P_1 is positive at the top vapor interface and negative at the bottom, indicating that CO and OH groups tend to point into the liquid. This orientation allows these polar groups to form intermolecular HBs. Our result agrees with that on glycerol[18] for which surface molecules expose the non-polar CH_x groups to air and point their CO and OH groups down or sideways to maximize the number of HBs.

Figure 6c and 6d characterize the backbone orientation using two order parameters: $P_1 = <\cos\theta>$ and $P_2 = <\frac{3}{2}\cos^2\theta - \frac{1}{2}>$, where θ is the angle between the C1-C5 vector and the surface normal. At the very edge of the film, P_2 is negative, meaning the backbone tends to lie flat on the surface. Deeper into the film, P_2 becomes positive, indicating the backbone tends to be vertical to the surface (parallel or antiparallel to z). The peak value of P_2 (0.25) corresponds to an average value of θ = 45º, slightly smaller than the magic angle of 55º for random orientation. Interestingly, for the C1-C5 vector, P_1 is a negative peak at the top of the film and a positive peak at the bottom. This means the C1-C5 vector tends to point towards the vapor, that is, a surface molecule tends to have its C5 end up (close to the vapor phase) and C1 end down (buried in the liquid phase). This tendency arises because the C1 and C5 ends are inequivalent. The C5 end has a bent CO group relative to the carbon chain and the molecule has lower energy if the C5 end is placed near the vapor phase, thus exposing the hydrophobic CH_2 group to the vapor phase and burying the polar CO group in the liquid to make hydrogen bonds, as observed for glycerol.[18] Together, the simulation results show that at the liquid/vapor interface, the molecules tend to be vertical with the polar CO and OH groups pointing downward (into the bulk) and with the C5 end pointing up (toward vapor). This structure maximizes the number of HBs per molecule, consistent with the nearly constant HB probability across the film (Figure 6a).

Based on the experimental and simulation results, we explain the fast, polymorph-selective nucleation at the liquid/vapor interface of D-arabitol as follows. Because surface molecules tend toward vertical orientation with the C5 end pointing up to maximize the number of HBs, the local structure is similar to the layered HB structure in Form II, and dissimilar to the 3D HB network in Form I. As a result, the surface molecular packing promotes the nucleation of Form II but not Form I. This explanation is

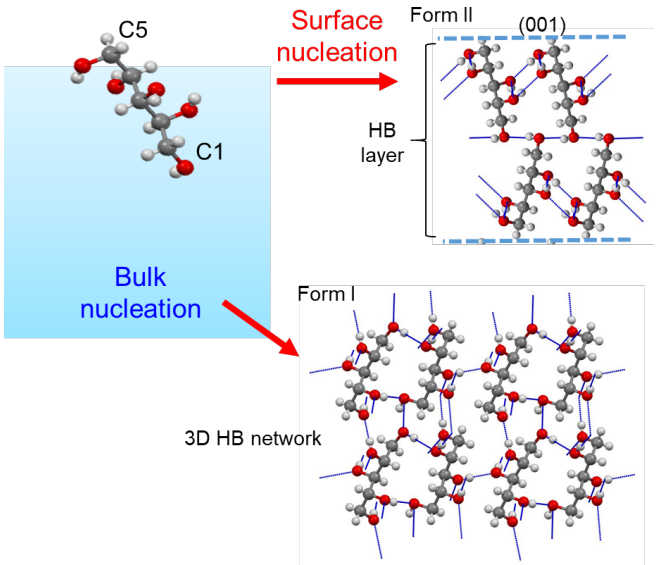

Figure 7. Surface-enhanced nucleation with polymorphic selection.

illustrated in Figure 7. Because the hydrogen-bonded layers are parallel to the (001) plane, our model immediately explains the preferred orientation of surface-nucleated crystals. Our model also explains the ability of a surface-active impurity (e.g., PVP; see Figure 5) to inhibit surface nucleation: the impurity is enriched in the surface layer, diluting the solvent molecules and modifying the local structure. This in turn disrupts the surface nucleation process. Because of mirror symmetry, the mechanism above applies equally to L-arabitol, thus explaining the same phenomenon observed for the enantiomer. We attribute the larger surface enhancement of nucleation with cooling (Figure 4b) to the increase of surface ordering. The rise of surface order with cooling is consistent with the literature results on the Lennard-Jones system[21] and liquid octane[19], and with our simulation results conducted at 400 K and 500 K (Figure S3). As Figure 4b shows, Kuhn et al.'s result on water aerosols also indicates a rising J_s/J_v ratio with cooling. This suggests that surface nucleation might be more easily detected at low temperatures.

Conclusions

We have observed that crystal nucleation is vastly faster on the surface of the molecular liquid D-arabitol than in the bulk, by 12 orders of magnitude on the per-molecule basis. Surface nucleation selects a different polymorph (II) than bulk nucleation (I). To our knowledge, this is the first time surface and bulk nucleation rates have been independently measured in the same system, revealing a huge difference between the two. This phenomenon is a consequence of the similarity of the surface molecular packing to the structure of the surface-nucleating polymorph. The mirror image of D-arabitol, L-arabitol, shows an identical phenomenon, strengthening our conclusion. We find that the surface enhancement effect intensifies with cooling.

Given the common occurrence of surface reconstruction, the surface effect on nucleation and polymorphism is potentially a general phenomenon. The phenomenon is expected if a slow-nucleating polymorph in the bulk has a structure that resembles the molecular organization at the liquid/vapor interface. The ability for surface nucleation to select a different polymorph from the bulk provides an intriguing avenue to expand the tools for polymorph discovery and control.[28,40] Besides arabitol, alkanes provide a possible example of polymorph selection by surface nucleation where the surface-frozen monolayer presumably nucleates the rotator phase in the bulk with little

supercooling.[12] Even in bulk liquids and glasses, surface nucleation could play a role through free surfaces created by bubbles[41] and fractures.[11, 42] Surface nucleation might be more easily observed in systems of large surface-to-volume ratios (e.g., nano-droplets[8, 9]) and at low temperatures, since the ratio J_s/J_v increases with cooling (Figure 4b). For liquids of multiple components, the surface layer can be enriched or depleted of certain components depending on surface tension. This effect will likely play a role in the surface crystallization of multi-component liquids.[43-45] It is of interest to learn whether the CNT provides a good foundation for understanding these phenomena.

Materials and Methods

D-arabitol and L-arabitol were purchased from Sigma-Aldrich and used either as received or after recrystallization, with no significant difference observed between as-received and recrystallized materials. For recrystallization, the material was dissolved in ethanol-water (15:1) at 350 K and the hot solution was filtered. The solution was cooled to room temperature and seeded with D- or L-arabitol crystals. After complete crystallization, the mother liquor was decanted, and the crystals were washed three times with the solvent and dried under vacuum.

To investigate surface crystallization, a liquid film with an open surface was prepared by spreading a liquid of D-arabitol at 403 K on a heat-treated coverslip that facilitates spreading.[46] For comparison, bulk crystallization was investigated using a liquid film sandwiched between two coverslips. Briefly, in the one-stage method, crystals were allowed to form in a sample and the birth time of each crystal was calculated from the current time and the growth rate. This method was used for temperatures at which crystal growth was relatively fast. If crystal growth was slow, a two-stage method was used in which a sample was held at a low temperature for different times and heated to a high temperature to allow the nuclei to grow and be counted. For each measurement, an open-surface sample was kept in the nitrogen-purged chamber of a temperature-controlled microscope stage (Linkam THMS).

X-ray Photoelectron Spectroscopy (XPS) was performed using a Thermo Scientific K-Alpha X-ray Photoelectron Spectrometer with a monochromatic Al Kα (1486.6 eV) source. Samples of D-arabitol doped with PVP K30 were prepared by melting the material, degassing at 403 K, and quenching to room temperature. XPS data were collected at 297 K in vacuum (10^{-5} Pa). The surfaces of the non-conductive samples were neutralized using an electron flood gun. The beam

size was 400 μm. A survey scan was performed for multiple elements at a step size of 1 eV and passing energy of 200 eV. High-resolution scans for the elements of interest (C, N, O) were performed at a step size of 0.1 eV and passing energy of 50 eV. The binding energy was calibrated by shifting the observed carbon peak (C 1s) to 285.0 eV. The baseline for peak area integration was obtained using a smart baseline function in Avantage Data System. The peak areas of N and O were used to calculate the surface weight percent of PVP K30 (w_p) as follows:

$$w_p = \frac{5R_{N/O} \times M_p}{5R_{N/O} \times M_p + (1 - R_{N/O})M_a} \times 100\%$$

where $R_{N/O}$ is the observed N/O atomic ratio after normalizing each peak area with the Relative Sensitivity Factor, M_a is the molecular weight of D-arabitol, and M_p is the monomer molecular weight of PVP K30. This method has been validated against chemically pure compounds[38] and against PVP K30, for which the measured N/O ratio is 1.017 (0.038) in agreement with the theoretical value (1).

Differiancial Scanning Calorimetry (DSC) was performed with a TA Q2000 under 50 mL/min N_2 purge. Each sample was 2-10 mg placed in an aluminum pan. Single Crystal X-Ray Diffraction was used to solve the structure of D-arabitol Form II. A single crystal of Form II was grown as follows: melt the as-purchased crystals on a coverslip to form isolated droplets, cool the droplets to 303 K, nucleate the sample at 303 K for several seconds, crystallize the droplets at 343 K in 2 min (some of which contained Form II, identifiable on sight), select a Form II polycrystalline assembly, raise the temperature to melt all but one crystal as a seed, and grow the seed at 343 K to a single crystal, consuming all the liquid in the droplet. The process may be repeated to improve crystal quality. The resulting crystal has adequate size and quality for structural solution X-ray diffraction (Bruker APEXII diffractometer; see Supporting Information and deposited cif file for details).

Molecular dynamics (MD) simulations of D-arabitol were performed at 400 K and 0.1 MPa. The force field (FF) was modified AMBER BCFF (Table S3 and S4). BCFF has performed well for glycerol (a smaller polyol)[34] and we have modified it to ensure that the molecular conformations in the liquid state approximately match those observed in crystals (see below). As a validation of the FF, we tested the stability of the experimental crystal structures and found that the experimental structures were reproduced by the MD simulation (Table S5). For bulk-liquid

simulations, a cubic box containing 800 molecules was used with periodic boundary conditions. To study a liquid with free surfaces, a box containing an equilibrated bulk system with 1600 molecules was extended in the z-direction to create a vacuum above and below the liquid film. The box size with 1600 molecules yielded a film thick enough to avoid any thin film effect; this was confirmed by (1) surface energy convergence tests and (2) comparing the structure with a film half as thick (with 800 molecules) and finding no significant difference (Figure S4). All simulations were performed using the GROMACS package[47, 48] on a high-performance computing cluster.[49] A timestep of 2 fs was used.[50] The simulation was conducted for 140 ns for both the bulk system and the free-standing film so that the mean square displacement of the molecules exceeded twice the molecular size and that the energy equilibrium was achieved. The temperature was controlled with a V-rescale style thermostat[51] and the pressure with a Berendsen barostat. The coupling time was 0.1 ps for the thermostat and 1 ps for the barostat. The following criteria were used for hydrogen bonds: O…O distance is between 2.5-3.5 Å and the H-O…O angle is less than 30°.

Supporting Information

Structural parameters of arabitol crystals. Terminal CO orientations of linear polyols based on survey of the Cambridge Structural Database (CSD). Illustration of nucleation rate measurement using the development method. XPS scans of D-arabitol samples containing PVP K30. MD simulations parameters and results.

Acknowledgements

We thank AbbVie Inc. and the Wisconsin - Puerto Rico Partnership for Research and Education in Materials (NSF DMR-1827894) for supporting this work. BW and QL thank the support from the National Science Foundation through the University of Wisconsin Materials Research Science and Engineering Center (NSF DMR-1720415). The Bruker SMART APEX2 was purchased by the UW–Madison Department of Chemistry with a portion of a generous gift from Paul J. and Margaret M. Bender. We thank Ilia A. Guzei for his support on the single-crystal X-ray diffraction study.

Disclosure

AbbVie participated in study design, research, data collection, analysis and interpretation of data, writing, reviewing, and approving the publication. X.Y., Q.L., B.W., J.Y., M.M.A., I.A.G., and L.Y. have no additional conflicts of interest to report. C.S. was an employee, G.G.Z.Z. is an employee of AbbVie and may own AbbVie stock.

Author Information

Corresponding Authors

Lian Yu - School of Pharmacy and Department of Chemistry, University of Wisconsin-Madison, Madison, WI, 53705, USA. Telephone: 608-263-2263. E-mail: lian.yu@wisc.edu.

Geoff G. Z. Zhang - Drug Product Development, Research and Development, AbbVie Inc., North Chicago, IL, 60064, USA. Telephone: 847-937-4702. E-mail: Geoff.GZ.Zhang@abbvie.com.

Authors

Xin Yao - School of Pharmacy, University of Wisconsin-Madison, Madison, WI, 53705, USA

Qitong Liu - Civil & Environmental Engineering, University of Wisconsin-Madison, Madison, WI, 53705, USA

Bu Wang - Civil & Environmental Engineering, University of Wisconsin-Madison, Madison, WI, 53705, USA

Junguang Yu - School of Pharmacy, University of Wisconsin-Madison, Madison, WI, 53705, USA

Michael M. Aristov - Department of Chemistry, University of Wisconsin-Madison, Madison, WI, 53705, USA

Chenyang Shi - Drug Product Development, Research and Development, AbbVie Inc., North Chicago, IL, 60064, USA. Current address: Data Science Consulting, Tiger Analytics, Santa Clara, CA, 95054, USA

References

1. Nielsen, M. H.; Aloni, S.; De Yoreo, J. J., In situ TEM imaging of CaCO3 nucleation reveals coexistence of direct and indirect pathways. *Science* **2014,** *345* (6201), 1158-1162.
2. Van Driessche, A. E.; Van Gerven, N.; Bomans, P. H.; Joosten, R. R.; Friedrich, H.; Gil-Carton, D.; Sommerdijk, N. A.; Sleutel, M., Molecular nucleation mechanisms and control strategies for crystal polymorph selection. *Nature* **2018,** *556* (7699), 89-94.
3. Walsh, M. R.; Koh, C. A.; Sloan, E. D.; Sum, A. K.; Wu, D. T., Microsecond simulations of spontaneous methane hydrate nucleation and growth. *Science* **2009,** *326* (5956), 1095-1098.
4. Zhou, J.; Yang, Y.; Yang, Y.; Kim, D. S.; Yuan, A.; Tian, X.; Ophus, C.; Sun, F.; Schmid, A. K.; Nathanson, M., Observing crystal nucleation in four dimensions using atomic electron tomography. *Nature* **2019,** *570* (7762), 500-503.
5. DeMott, P. J.; Prenni, A. J.; Liu, X.; Kreidenweis, S. M.; Petters, M. D.; Twohy, C. H.; Richardson, M.; Eidhammer, T.; Rogers, D., Predicting global atmospheric ice nuclei distributions and their impacts on climate. *Proceedings of the National Academy of Sciences* **2010,** *107* (25), 11217-11222.
6. Sosso, G. C.; Chen, J.; Cox, S. J.; Fitzner, M.; Pedevilla, P.; Zen, A.; Michaelides, A., Crystal nucleation in liquids: Open questions and future challenges in molecular dynamics simulations. *Chemical reviews* **2016,** *116* (12), 7078-7116.
7. Bartels-Rausch, T., Ten things we need to know about ice and snow. *Nature* **2013,** *494* (7435), 27-29.
8. Nam, H.-S.; Hwang, N. M.; Yu, B.; Yoon, J.-K., Formation of an icosahedral structure during the freezing of gold nanoclusters: surface-induced mechanism. *Physical review letters* **2002,** *89* (27), 275502.
9. Mendez-Villuendas, E.; Bowles, R. K., Surface nucleation in the freezing of gold nanoparticles. *Physical Review Letters* **2007,** *98* (18), 185503.
10. Li, T.; Donadio, D.; Ghiringhelli, L. M.; Galli, G., Surface-induced crystallization in supercooled tetrahedral liquids. *Nature materials* **2009,** *8* (9), 726-730.
11. Descamps, M.; Dudognon, E., Crystallization from the amorphous state: nucleation–growth decoupling, polymorphism interplay, and the role of interfaces. *Journal of pharmaceutical sciences* **2014,** *103* (9), 2615-2628.
12. Sirota, E., Supercooling, nucleation, rotator phases, and surface crystallization of n-alkane melts. *Langmuir* **1998,** *14* (11), 3133-3136.
13. Last, J. A.; Hooks, D. E.; Hillier, A. C.; Ward, M. D., The physicochemical origins of coincident epitaxy in molecular overlayers: Lattice modeling vs potential energy calculations. *The Journal of Physical Chemistry B* **1999,** *103* (32), 6723-6733.
14. Weissbuch, I.; Lahav, M.; Leiserowitz, L., Toward stereochemical control, monitoring, and understanding of crystal nucleation. *Crystal growth & design* **2003,** *3* (2), 125-150.
15. Mitchell, C. A.; Yu, L.; Ward, M. D., Selective nucleation and discovery of organic polymorphs through epitaxy with single crystal substrates. *Journal of the American Chemical Society* **2001,** *123* (44), 10830-10839.
16. Magnussen, O.; Ocko, B.; Regan, M.; Penanen, K.; Pershan, P. S.; Deutsch, M., X-ray reflectivity measurements of surface layering in liquid mercury. *Physical review letters* **1995,** *74* (22), 4444.
17. Regan, M.; Kawamoto, E.; Lee, S.; Pershan, P. S.; Maskil, N.; Deutsch, M.; Magnussen, O.; Ocko, B.; Berman, L., Surface layering in liquid gallium: An X-ray reflectivity study. *Physical review letters* **1995,** *75* (13), 2498.
18. Oh-e, M.; Yokoyama, H.; Baldelli, S., Structure of the glycerol liquid/vapor interface studied by sum-frequency vibrational spectroscopy. *Applied physics letters* **2004,** *84* (24), 4965-4967.
19. Haji-Akbari, A.; Debenedetti, P. G., Thermodynamic and kinetic anisotropies in octane thin films. *The Journal of chemical physics* **2015,** *143* (21), 214501.

20. Bishop, C.; Thelen, J. L.; Gann, E.; Toney, M. F.; Yu, L.; DeLongchamp, D. M.; Ediger, M. D., Vapor deposition of a nonmesogen prepares highly structured organic glasses. *Proceedings of the National Academy of Sciences* **2019,** *116* (43), 21421-21426.
21. Haji-Akbari, A.; Debenedetti, P. G., The effect of substrate on thermodynamic and kinetic anisotropies in atomic thin films. *The Journal of chemical physics* **2014,** *141* (2), 024506.
22. Zhu, L.; Brian, C.; Swallen, S.; Straus, P.; Ediger, M.; Yu, L., Surface self-diffusion of an organic glass. *Physical Review Letters* **2011,** *106* (25), 256103.
23. Turnbull, D., Kinetics of heterogeneous nucleation. *The Journal of Chemical Physics* **1950,** *18* (2), 198-203.
24. Vrbka, L.; Jungwirth, P., Homogeneous freezing of water starts in the subsurface. *The Journal of Physical Chemistry B* **2006,** *110* (37), 18126-18129.
25. Haji-Akbari, A.; DeFever, R. S.; Sarupria, S.; Debenedetti, P. G., Suppression of sub-surface freezing in free-standing thin films of a coarse-grained model of water. *Physical Chemistry Chemical Physics* **2014,** *16* (47), 25916-25927.
26. Haji-Akbari, A.; Debenedetti, P. G., Computational investigation of surface freezing in a molecular model of water. *Proceedings of the National Academy of Sciences* **2017,** *114* (13), 3316-3321.
27. Haji-Akbari, A.; Debenedetti, P. G., Perspective: Surface freezing in water: A nexus of experiments and simulations. *The Journal of chemical physics* **2017,** *147* (6), 060901.
28. Bernstein, J., *Polymorphism in Molecular Crystals 2e*. International Union of Crystal: 2020; Vol. 30.
29. Lewis, D.; Smith, D., Sugar alcohols (polyols) in fungi and green plants. I. Distribution, physiology and metabolism. *The New Phytologist* **1967,** *66* (2), 143-184.
30. Back, J. F.; Oakenfull, D.; Smith, M. B., Increased thermal stability of proteins in the presence of sugars and polyols. *Biochemistry* **1979,** *18* (23), 5191-5196.
31. Gunasekara, S. N.; Pan, R.; Chiu, J. N.; Martin, V., Polyols as phase change materials for surplus thermal energy storage. *Applied Energy* **2016,** *162*, 1439-1452.
32. Kopf, J.; Morf, M.; Zimmer, B.; Köll, P., Kristall-und molekülstruktur von d-arabinitol. *Carbohydrate research* **1991,** *218*, 9-13.
33. Jeffrey, G.; Kim, H., Conformations of the alditols. *Carbohydrate Research* **1970,** *14* (2), 207-216.
34. Huang, C.; Chen, Z.; Gui, Y.; Shi, C.; Zhang, G. G.; Yu, L., Crystal nucleation rates in glass-forming molecular liquids: D-sorbitol, D-arabitol, D-xylitol, and glycerol. *The Journal of chemical physics* **2018,** *149* (5), 054503.
35. Duft, D.; Leisner, T., Laboratory evidence for volume-dominated nucleation of ice in supercooled water microdroplets. *Atmospheric Chemistry and Physics* **2004,** *4* (7), 1997-2000.
36. Kuhn, T.; Earle, M.; Khalizov, A.; Sloan, J., Size dependence of volume and surface nucleation rates for homogeneous freezing of supercooled water droplets. *Atmospheric Chemistry and Physics* **2011,** *11* (6), 2853-2861.
37. Yao, X.; Huang, C.; Benson, E. G.; Shi, C.; Zhang, G. G.; Yu, L., Effect of polymers on crystallization in glass-forming molecular liquids: equal suppression of nucleation and growth and master curve for prediction. *Crystal Growth & Design* **2019,** *20* (1), 237-244.
38. Yu, J.; Li, Y.; Yao, X.; Que, C.; Huang, L.; Hui, H.-W.; Gong, Y. G.; Yu, L., Surface Enrichment of Surfactants in Amorphous Drugs: An X-Ray Photoelectron Spectroscopy Study. *Molecular pharmaceutics* **2022,** *19* (2), 654-660.
39. Jahn, D. A.; Akinkunmi, F. O.; Giovambattista, N., Effects of temperature on the properties of glycerol: A computer simulation study of five different force fields. *The Journal of Physical Chemistry B* **2014,** *118* (38), 11284-11294.
40. Bauer, J.; Spanton, S.; Henry, R.; Quick, J.; Dziki, W.; Porter, W.; Morris, J., Ritonavir: an extraordinary example of conformational polymorphism. *Pharmaceutical research* **2001,** *18* (6), 859-866.

41. Wohlgemuth, K.; Kordylla, A.; Ruether, F.; Schembecker, G., Experimental study of the effect of bubbles on nucleation during batch cooling crystallization. *Chemical Engineering Science* **2009,** *64* (19), 4155-4163.
42. Su, Y.; Yu, L.; Cai, T., Enhanced crystal nucleation in glass-forming liquids by tensile fracture in the glassy state. *Crystal Growth & Design* **2018,** *19* (1), 40-44.
43. Shpyrko, O. G.; Streitel, R.; Balagurusamy, V. S.; Grigoriev, A. Y.; Deutsch, M.; Ocko, B. M.; Meron, M.; Lin, B.; Pershan, P. S., Surface crystallization in a liquid AuSi alloy. *Science* **2006,** *313* (5783), 77-80.
44. Sutter, P. W.; Sutter, E. A., Dispensing and surface-induced crystallization of zeptolitre liquid metal-alloy drops. *Nature materials* **2007,** *6* (5), 363-366.
45. Lü, Y.; Chen, M., Surface layering-induced crystallization of Ni–Si alloy drops. *Acta materialia* **2012,** *60* (11), 4636-4645.
46. Zhang, D.; Gao, N.; Yan, W.; Luo, W.; Zhang, L.; Zhao, C.; Zhang, W.; Liu, D., Heat induced superhydrophilic glass surface. *Materials Letters* **2018,** *223*, 1-4.
47. Berendsen, H. J.; van der Spoel, D.; van Drunen, R., GROMACS: a message-passing parallel molecular dynamics implementation. *Computer physics communications* **1995,** *91* (1-3), 43-56.
48. Abraham, M. J.; Murtola, T.; Schulz, R.; Páll, S.; Smith, J. C.; Hess, B.; Lindahl, E., GROMACS: High performance molecular simulations through multi-level parallelism from laptops to supercomputers. *SoftwareX* **2015,** *1*, 19-25.
49. This research was performed using the compute resources and assistance of the UW-Madison Center For High Throughput Computing (CHTC) in the Department of Computer Sciences. The CHTC is supported by UW-Madison, the Advanced Computing Initiative, the Wisconsin Alumni Research Foundation, the Wisconsin Institutes for Discovery, and the National Science Foundation, and is an active member of the Open Science Grid, which is supported by the National Science Foundation and the U.S. Department of Energy's Office of Science.
50. Hess, B., P-LINCS: A parallel linear constraint solver for molecular simulation. *Journal of chemical theory and computation* **2008,** *4* (1), 116-122.
51. Bussi, G.; Donadio, D.; Parrinello, M., Canonical sampling through velocity rescaling. *The Journal of chemical physics* **2007,** *126* (1), 014101.

TOC figure: